Proceedings of the 3rd International
IEEE EMBS Conference on Neural Engineering
Kohala Coast, Hawaii, USA, May 2-5, 2007

Spatially Selective Filter Design for High-Resolution EMG Arrays

John David Quartararo and Edward A. Clancy*, *Senior Member, IEEE*

***Abstract*—A new technique for designing EMG spatial filters with optimized spatial selectivity is described. Simulations were used to model an action potential (AP) as a tripole source within the muscle, and to calculate the voltage induced at an array of surface monopolar electrodes. Next, a map of desired spatial filter output voltages was created as a function of the location of an AP beneath the array. Linear least squares was used to solve for the filter weights which optimally matched the desired filter outputs to those resulting from the tripole model. The optimized filters were found to be consistently superior to the conventional normal double differentiating filter. Selectivity was a function of the simulated inter-electrode spacing and the number of electrodes in the array.**

I. Introduction

SURFACE electromyogram (EMG) arrays may be useful in the diagnosis and study of many neurogenic/myogenic disorders [15]. Surface electrode arrays are noninvasive, eliminating the patient discomfort of inserted needles, and can track the propagation of a motor unit action potential (MUAP), allowing estimation of the muscle fiber conduction velocity (MFCV). Irregularities in MFCV can be a symptom of many disorders, including McArdle's disease [22]. A key to unlocking diagnostic information is the ability to decompose the composite EMG interference pattern into the constituent firings of each MUAP. Surface electrodes typically have poorer spatial resolution than needle electrodes, resulting in the simultaneous recording of more MUAPs — a detriment to decomposition. Additionally, the surface EMG signal is distorted compared to indwelling EMG [11].

Spatial filtering has been shown to be an invaluable tool in surface decomposition by limiting the number of superimposed MUAPs contributing to the analyzed signal [5], [18]. Reucher *et al.* [18], [19] investigated bipolar and NDD (normal double difference, a.k.a. "Laplacian") configurations with respect to their ability to increase selectivity. Other spatial filters (e.g., 2nd order inverse binomial, 4th order inverse binomial, inverse rectangle) [5] have been investigated and the 2nd order inverse binomial filter was shown to be well-adapted to non-invasive surface EMG. Farina and Rainoldi [8] created an optimal spatial filter by introducing an analytic model of the muscle and skin and finding an inverse transfer function. In this paper, a new approach to spatial filter design is presented.

Supported in part by the National Institute of Neurological Disorders and Stroke (NINDS), USA under grant NS44872; and a Research Advancement Program grant from Worcester Polytechnic Institute (WPI).

J. D. Quartararo is with the Department of Electrical and Computer Engineering, WPI, Worcester, MA 01609 (e-mail: johndq@gmail.com).

*E. A. Clancy (corresponding author) is with the Department of Electrical and Computer Engineering, and the Department of Biomedical Engineering, WPI, Worcester, MA 01609 (e-mail: ted@wpi.edu).

II. Methods

A. *Tripole Model*

Surface potentials were simulated as from a rectangular array of point electrodes due to MUAPs located within the muscle tissue, using MATLAB (The Mathworks, Natick, MA, USA). All electrodes were assumed to be located on one side of the innervation region. Muscle fiber de-/re-polarization processes were realized as a current tripole [2], [20] whose transmembrane ionic currents (I_m, m=1,2,3) [23] were induced by the MUAP as it propagated down the muscle fiber with conduction velocity v, typically in the range of 3–5 m/s [6]. The surface potential at a point on the skin was calculated as [23]:

$$V_k = \sum_{m=1}^{3} \frac{I_m}{4\pi \cdot \sigma \cdot d_{km}} \tag{1}$$

where I_m (Amps) is the point current value of the m^{th} pole, d_{km} (m) is the distance between the m^{th} pole and the point of measurement for the k^{th} electrode, V_k (Volts) is the voltage induced at the k^{th} electrode, and σ (Siemens/m) is the conductivity of the volume conductor. It was assumed that the conductive media between the tripole source and each electrode was isotropic, homogeneous and of infinite extent. The tissue conductivity σ was set to 0.5 Siemens/m.

The electrode array was situated at depth $z = 0$, where the x-y plane is the surface of the skin, and the $-z$ direction extends down into the skin. The $+x$ direction is the direction of AP propagation. The distance in the x direction between the middle and leading pole was 2 mm, and the distance between the middle and trailing pole was 4 mm [19]. The leading point-source current value was set to 12 μA (I_1), the central source value to -18 μA (I_2), and the trailing source value to 6 μA (I_3) [18], [19]. The location of the central source value was used as the gross location of the tripole.

B. *Least Squares Optimization Method*

Spatial filtering is accomplished by weighting each monopolar electrode voltage and summing to yield a single output signal: $V_{Filter}(l) = \sum_{k=1}^{K} e_k(l) \cdot w_k$, where $e_k(l)$ is the simulated monopolar voltage from the k^{th} electrode from measurement l, w_k is the filter weight of the k^{th} electrode and K is the number of electrodes. The problem at hand is to optimize the weights such that a small region of the muscle

tissue is emphasized (i.e., contributes to the spatially filtered voltage), while the remaining volume is de-emphasized.

To create a spatially selective filter, consider fixing the tripole at numerous positions on an *x*, *y*, *z* grid within the muscle. The simulator is then used to find the corresponding monopolar voltages induced at each array electrode from each tripole position. Next, a map of desired spatial filter output voltages [$V_{Desired}(x,y,z)$] is created, one voltage corresponding to each tripole location within the grid. These desired voltages are set to zero at locations where the tripole should be attenuated and set to one where the tripole should contribute to the spatially filtered signal. The locations set to one represent the volume of focus for the array. In practice, the desired voltages were set to ones within a single column along the *z* axis, from 1 mm below a focal point up to the focal point (i.e., along a range of the *z* axis). Unless noted otherwise, this focal column was situated at the center of the *x*–*y* plane. Thus, the *z*-axis depth of the focus was sufficient to specify the desired voltage pattern.

For the l^{th} AP location within the muscle, we seek to select weights to minimize the error in:

$$V_{Desired}(l) = w_1 \cdot e_1(l) + w_2 \cdot e_2(l) + ... + w_K \cdot e_K(l) + Error_l$$

where $Error_i$ is the error between the desired spatially filtered voltage and that achieved for this tripole location. If *L* such *x*, *y*, *z* grid locations are tabulated, a set of *L* equations in the weights is formed. Since all of the desired voltages [$V_{Desired}(l)$] and monopolar voltages [$e_k(l)$] are known, selection of the spatial filter weights (w_k) to minimize the mean squared error results in the conventional linear LS problem [10], [12], [14], [21]. We solved the least squares problem using the Moore-Penrose pseudoinverse [10], [21], computed using singular value decomposition [14] with a tolerance level of $0.1*N_o*eps*L$ (N_o is the norm of the product of the design matrix transpose and the design matrix, and *eps* is the smallest floating point number).

For all designs, the evaluation grid ranged from –20 to +20 mm in the *x* and *y* directions (0.2 mm increment), and from the focal point to 1 mm below the focal point in the *z* direction (0.1 mm increment). Two focal depths were used, 4 and 7 mm. Other depths were investigated and produced results consistent with those reported herein. Simulations were run for interelectrode spacings from 0.5 to 5 mm (0.5 mm increment), using a 15 x 15 electrode array; and square arrays with varying numbers of electrodes (3^2, 5^2, 7^2, 9^2, 11^2) with a constant 2.5 mm interelectrode spacing. The optimized filters were compared to the monopolar and NDD filter performances using two metrics of selectivity, discussed below. The NDD filter consists of five electrodes arranged in the shape of a cross: the center electrode has a weight of –4, while the remaining electrodes have a weight of one. The central NDD electrode and the monopolar electrode were located directly above the focal region.

C. *Quantitative Spatial Selectivity Metrics*

Two metrics were calculated after designing each filter. For the first metric, the tripole source was repeatedly located throughout a grid in the *x*-*y* plane, at the fixed focal depth in the *z* axis at which that filter had been designed. At each location, the voltage produced by the spatial filter was computed, yielding a 3D contour map (or, action potential sensitivity map). Maps with a sharper peak correspond to filters with higher selectivity — they are more sensitive to AP voltages arising from a confined volume within the muscle. To quantify this selectivity, the distance from the peak voltage to the 3 dB drop (amplitude) was found along the *x* and *y* axes in the positive and negative directions and each were averaged, respectively. These two distances formed the semi-major and semi-minor axes of an ellipse, whose area was taken as the metric of spatial selectivity; a smaller area implying higher selectivity.

The ability to suppress APs that are slightly offset from the focus of selectivity was used as the second metric for evaluating filter performance [8]. Two traveling APs were simultaneously simulated as a function of time. One AP passed through the array center (the filter's focal point) along the *x* axis while the other traveled along a parallel path with a slight offset in the *y* direction. Both APs were at the same depth and had the same conduction velocity. In addition, the second AP was time-delayed so that its

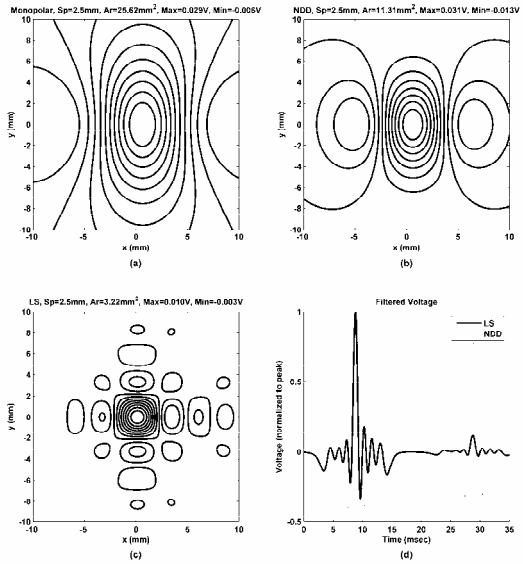

Fig. 1. Top (left, right) and bottom left show action potential sensitivity maps using a 15 by 15 array, interelectrode spacing of 2.5 mm and an action potential depth of 7 mm. Each contour plot contains 10 contour lines. Top left shows results from a monopolar filter (3 dB selectivity of 25.62 mm^2). Top right shows results from an NDD filter (3 dB selectivity of 11.31 mm^2). Bottom left shows results from a least squares filter (3 dB selectivity of 3.22 mm^2). Bottom right shows a time-voltage plot used to determine the second selectivity metric (ratio of amplitudes) for two action potentials separated by 2 mm (action potential depth of 7 mm). Solid line is the array output for the least squares filter. Dash line is the array output for the NDD filter. The amplitude of both time plots is normalized to the maximum value of their respective plot. The least squares filter suppresses the second action potential response to 12.1% of the first action potential, while the NDD only suppresses to 77.9%.

TABLE I
THREE DB AREA SELECTIVITY (MM^2) FOR NDD AND LS FILTERS FOR VARIOUS LEVELS OF GAIN ERROR IN FILTER WEIGHTS, DEPTH OF 7 MM, 100 TEST CASES EACH

Gain Error	NDD		LS	
	mean	std	mean	std
0%	11.31	0	3.22	0
1%	11.31	0.2	9.02	6.49
2%	11.33	0.31	22.14	11.79
3%	11.29	0.45	26.51	12.50
4%	11.32	0.68	†	†
5%	11.28	0.81	†	†
6%	11.24	1	†	†

† Three dB area larger than evaluation grid dimensions.

contribution to the overall voltage recording was not superimposed on the first AP. The ratio of the second AP's peak amplitude to that of the first was taken as the second metric of spatial selectivity. A low ratio implies that the filter attenuates the second firing well, while a higher value implies less selectivity.

D. Filter Sensitivity

To evaluate filter sensitivity to the accuracy of the filter weights, spatial filter weights were each randomly perturbed and the 3 dB area metric re-computed. An independent, unit-mean and uniformly distributed random value was multiplied by each weight. To represent a 1% gain tolerance, the random number ranged between 0.99 and 1.01. Similarly, gain tolerances up to 6% were investigated. This test was repeated 100 times for each condition, and the mean and standard deviation 3 dB area of sensitivity reported. A lower mean area implies better selectivity, and a lower standard deviation implies more robustness to noise.

III. RESULTS

A. Optimized Spatial Filters

Fig. 1 shows representative results comparing the LS-based filters to conventional spatial filters. Fig. 2 shows results of the effect of various interelectrode spacings and numbers of electrodes on the 3 dB area selectivity. Selectivity increases as the interelectrode spacing reduces; the LS filter shows superior selectivity for the range of spacings investigated. The plot on the right shows that increasing the number of electrodes (i.e., increasing the area of coverage) leads to an increase in selectivity. This increase plateaus at 49 electrodes (7 x 7 configuration, 2.5 mm interelectrode distance). For comparison, the NDD filter has a selectivity of 5.48 mm^2 when the AP depth is 4 mm and 11.31 mm^2 when the AP depth is 7 mm. Beyond a 49 electrode array, increasing the number of electrodes did not increase the filter selectivity. However, smaller interelectrode distances (e.g., 0.5 mm) benefited from arrays as large as 25 x 25 and exhibited better selectivity.

The second metric of selectivity (ratio of 2nd peak amplitude to 1st) is plotted for various AP offsets in the y-direction in Fig. 3. The LS filter is consistently better at suppressing APs outside the volume of interest than the NDD filter. Similar results were found at a depth of 4 mm.

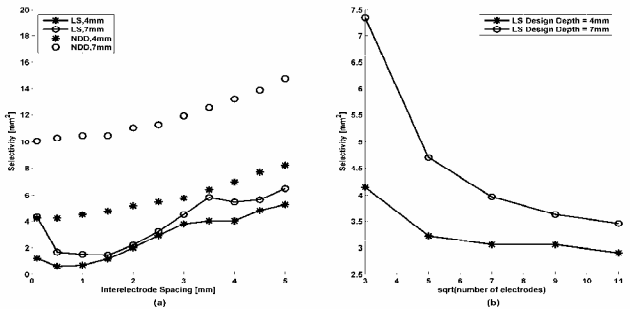

Fig. 2. Influence of number of electrodes and interelectrode spacing on 3 dB selectivity metric. Left plot shows the 3 dB selectivity versus interelectrode spacing for the least squares ("LS") and NDD filters for simulated action potentials at two different depths, using a 15 x 15 array. Right plot shows the 3 dB selectivity versus number of electrodes for the least squares ("LS") filter for simulated action potentials at two different depths. A square array with interelectrode spacing of 2.5 mm was used. Lines are an aid to the eye only.

B. Filter Sensitivity to Channel Noise/Gains

As shown in Table I, when the filter weights obtained from the LS filters were randomly perturbed by as little as 2–3%, the resultant 3 dB selectivity degraded unacceptably (i.e., worse than the NDD filter). The filters would be extremely sensitive to noise and imperfections in the component values within the electrode array hardware. The NDD filter exhibited consistent selectivity up to 6% gain error, with a small standard deviation. Similar results were found at a depth of 4 mm.

IV. DISCUSSION AND CONCLUSIONS

Our simulation results found that designing a spatial filter by optimizing selection of its weights to a desired filter output map produced a more spatially selective filter than

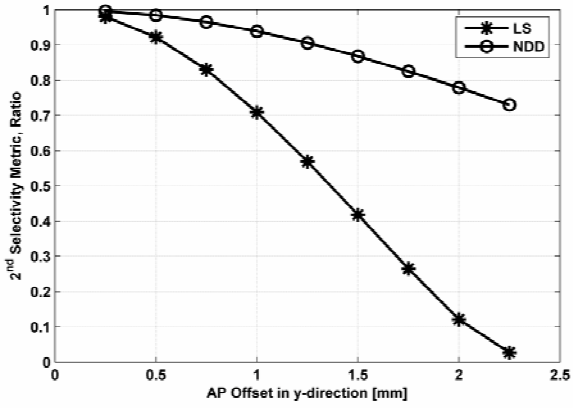

Fig. 3. Influence of action potential (AP) separation (i.e., offset distance) on ratio of peak amplitude (second metric of spatial selectivity). Plot shows the ratio of the distant AP peak to that of another AP traveling through the center of the electrode array, both at a depth of 7 mm for the least squares and NDD filters (LS filters designed for focal depth of 7 mm). Interelectrode distance is 2.5 mm with a 15 x 15 electrode array. Lines are an aid to the eye only.

existing conventional filters, based on our simulation model. However, we found that these spatial filters were overly sensitive to gain variations in the filter weights. Since channel-to-channel gain variations on the order of 1%–5% are inevitable within existing EMG hardware, this sensitivity must be avoided. Possible solutions to this problem include using a larger tolerance level in the Moore-Penrose pseudoinverse or other LS regularization strategies. Our preliminary analysis of such techniques suggests that higher robustness to gain variations can be achieved, at the expense of some filter selectivity. Alternatively, one can develop a data acquisition system with channel gain matching well below 1% error using software equalization [1].

The optimized spatial filters were a substantial improvement over conventional filters, as evaluated by this simulation model. For comparison, monopolar electrodes exhibited a 3 dB area of 25.62 mm^2; NDD electrodes with a 2.5 mm interelectrode spacing exhibited a 3 dB area of ~11.31 mm^2; optimized 15x15 arrays with 2.5 mm interelectrode spacings exhibited 3 dB areas of 3–7 mm^2, depending on the design parameters. Thus, the optimized filters provided a relative improvement over the NDD filter which is similar to the relative improvement that the NDD filter provides over the monopolar electrode. Selectivity was improved by a denser electrode array (down to an interelectrode spacing of 0.5 mm) and a larger electrode coverage area (up to some maximum area). These optimized filters may help reduce the number of superimpositions in the spatially filtered signal, thereby facilitating easier and more complete MU decomposition. Many such filters can be applied to develop multiple areas of focus beneath a single array, so as to decompose MUs located throughout the area covered by the array.

Note that the development of these optimized filters did not directly incorporate desired common mode rejection ratio (CMRR) characteristics of the spatial filter. Typically, the sum of the monopolar weights in a spatial filter is constrained to be zero so that common mode voltages are nulled. Fortunately, the weights created by our technique largely conform to this constraint inherently. Future research might look to more formally satisfy this CMRR constraint.

Our general optimization method can be expanded in the future to include several variants, each of which might improve the limitations of our existing model and method. First, we have used a rather simple model — perhaps overly simplistic — of the underlying physiology. More complete models [4], [7], [13] would better represent the potential distribution on the skin due to an AP source and produce more reliable indicators of performance with actual EMG signals [3]. Obviously, evaluation of spatial filters with actual EMG signals is imperative in the future, as well. Second, we have modeled the electrode potential as a point potential on the skin. Physical array electrodes are typically circular contacts, 1–2 mm in diameter. Models that account for electrode contact area can be used to more closely match the recorded electrode voltage. Third, we have used linear LS to optimize the parameters. Other system identification techniques exist to relate the recorded monopolar potentials to the desired spatially filtered outputs, including weighted LS and robust estimation. Fourth, we have created our desired map by assigning the value one to all locations associated with the area of focus and zeroes elsewhere. This technique is akin to digital design of ideal time-domain filters with neither a transition region nor a window [15], [16]. Spatial filtering might be improved by designing a less abrupt change at the interface between the focus area and the remaining tissue in the desired potential map.

REFERENCES

[1] E. A. Clancy, H. Xia, and M. V. Bertolina, "A Preliminary Report on the Use of Equalization Filters to Derive High Spatial Resolution Electrode Array Montages," *Proc. Int. Symp. Neuromusc. Assess. Eld. Worker (NEW)*, Torino, Italy, pp. 103–106, 2004.

[2] W. H. Craib, *J. Physiol.*, vol. 66, pp. 49–73, 1928.

[3] G. V. Dimitrov, C. Disselhorst-Klug, N. A. Dimitrova, E. Schulte E, and G. Rau, *J. Electromyogr. Kinesiol.*, vol. 13, pp. 125-138, 2003.

[4] N. A. Dimitrova, G. V. Dimitrov, and A. G. Dimitrov, *Med. Biol. Eng. Comput.*, vol. 39, no. 2, pp. 202–207, 2001.

[5] C. Disselhorst-Klug, J. Silny, and G. Rau, *IEEE Trans. Biomed. Eng.*, vol. 44, no. 7, pp. 567–574, 1997.

[6] D. Farina, R. Merletti, and D. Stegeman, "Biophysics of the Generation of EMG Signals," in *Electromyography: physiology, engineering, and noninvasive applications*, IEEE/John Wiley & Sons, Hoboken, NJ, 2004, pp. 81–105.

[7] D. Farina, L. Mesin, S. Martina, and R. Merletti, *IEEE Trans. Biomed. Eng.*, vol. 51, no. 3, pp. 415–426, 2004.

[8] D. Farina and A. Rainoldi, *Med. Eng. Physics*, vol. 21, pp. 487–496, 1999.

[9] S. Gabriel, R. W. Lau, and C. Gabriel, *Phys. Med. Biol.*, vol. 41, pp. 2251–2269, 1996.

[10] S. J. Leon, *Linear Algebra with Applications*, MacMillan Publishing Co., Inc., New York, 1980, pp. 307–310.

[11] L. Lindstrom, R. Magnusson, and I. Petersen, *Electromyography*, vol. 10, no. 4, pp. 341–356, 1970.

[12] Matlab® manual. Available: http://www.mathworks.com, 2005.

[13] L. Mesin and D. Farina, *IEEE Trans. Biomed. Eng.*, vol. 52, no. 12, pp. 1984–1993, 2005.

[14] W. H. Press, S. A. Teukolsky, W. T. Vetterling, and B. P. Flannery, *Numerical Recipes in C: The Art of Scientific Computing*, 2nd ed., Cambridge University Press, Cambridge, 1992, pp. 676–677.

[15] D. C. Preston and B. E. Shapiro, *Electromyography and Neuromuscular Disorders: Clinical-Electrophysiologic Correlations*, Butterworth-Heinemann, Boston, 1998, pp. 393, 503.

[16] J. G. Proakis and D. G. Manolakis, *Digital Signal Processing: Principles, Algorithms, and Applications*, 3rd ed., Prentice Hall, New Jersey, 1996, pp. 623–637.

[17] L. R. Rabiner, B. Gold, and M. C. McGonegal, *IEEE Trans. Audio Electro.*, vol. AU-18, pp. 83–106, 1970.

[18] H. Reucher, G. Rau, and J. Silny, *IEEE Trans. Biomed. Eng.*, vol. BME-34, no. 2, pp. 98–105, 1987.

[19] H. Reucher, G. Rau, and J. Silny, *IEEE Trans. Biomed. Eng.*, vol. BME-34, no. 2, pp. 106–113, 1987.

[20] P. Rosenfalck, *Acta. Physiol. Scand.*, Suppl. 321, pp. 1–168, 1969.

[21] G. Strang, *Linear Algebra and Its Applications*, Academic Press, NY, pp. 114, 137–145, 1980.

[22] M. Zwarts, G. Drost and D. Stegeman, *J. Electromyo. Kinesiol.*, vol.10, pp. 287–291, 2000.

[23] M. Zwarts and D. Stegeman, *Muscle Nerve*, vol. 28, pp. 1–17, 2003.